

***Ab initio* lattice-gas modeling of interstitial hydrogen diffusion in CuPd alloys**

Preeti Kamakoti and David S. Sholl*

*Department of Chemical Engineering, Carnegie Mellon University, Pittsburgh, Pennsylvania 15213, USA
and National Energy Technology Laboratory, Pittsburgh, Pennsylvania 15236, USA*

(Received 14 May 2004; revised manuscript received 20 August 2004; published 6 January 2005)

A comprehensive lattice-gas model has been developed to predict the diffusivities of dilute H in a wide range of structurally disordered fcc CuPd alloys with compositions greater than 47 at. % Pd. We used density functional theory to perform detailed calculations of H binding energies, vibrational frequencies, and activation barriers to local diffusion in two representative alloys having 52 and 74 at. % Pd. These data are used to parametrize all possible hopping rates between adjacent interstitial sites in a lattice model for the entire range of compositions. Kinetic Monte Carlo (KMC) simulations of this lattice model were used to calculate H tracer diffusivities as a function of alloy composition and temperatures ranging from 400 K to 1200 K. The results from these simulations are found to be in good agreement with available experimental data. We have also used KMC simulations to investigate the impact of short-range order on H diffusion in fcc CuPd alloys. The effects of short-range order are found to be small under the conditions of experimental interest.

DOI: 10.1103/PhysRevB.71.014301

PACS number(s): 66.30.Dn, 71.15.Mb

I. INTRODUCTION

Hydrogen is a vast fuel source.¹ There is a critical need for hydrogen in petroleum refining and petrochemical production as well as in energy-related applications such as fuel cells.² One significant technical challenge associated with hydrogen production and purification is the development of membrane technology that can withstand elevated temperatures and pressures.³ Many petrochemical processes can be enhanced by gas separation with membranes at operating conditions. Palladium-based membranes for hydrogen separation have been the focus of many studies because of their potential in hydrogen separation and purification reactions. Past research in the area of sulfur poisoning of membrane materials has shown that even minute concentrations of sulfur-containing compounds can rapidly deactivate Pd membranes.^{4–6} One route to possibly minimizing this undesirable effect is to examine Pd-based alloys as membrane materials.

Several recent studies have suggested that membranes made of CuPd alloys may have favorable properties such as increased sulfur resistance and good thermal resilience,^{7–9} and, therefore, offer an attractive alternative to pure Pd membranes. Molecular hydrogen permeates through metal membranes by catalytic dissociation on the membrane surface, subsequent diffusion of atomic H through interstitial sites of the metal, and finally recombinative desorption of H₂ on the downstream side of the membrane.¹⁰ This suggests that an ideal hydrogen-selective metal membrane should possess high catalytic activity for H₂ dissociation, high solubility, and rapid diffusion of interstitial H. To use alloy membranes most effectively, it would be useful to have methods that accurately model the dependence of these various processes on alloy composition. The goal of this work is to develop a robust model describing hydrogen diffusion in CuPd alloys under conditions relevant to membrane application—that is, at elevated temperatures and dilute H concentrations.

CuPd alloys occur in multiple bulk phases as the composition of Cu is varied.^{11,12} A disordered fcc phase occurs for

a wide range of alloy compositions including the region above 47 at. % Pd at all temperatures and all alloy compositions at temperatures greater than 773 K. For a range of compositions centered at 40 at. % Pd and temperatures less than 773 K, the stable phase is an ordered bcc phase. In this paper, we focus on fcc CuPd alloys, since this is the stable phase at high temperatures.

The diffusion of H in pure Pd and CuPd alloys has been discussed by Volkl and Alefield.¹³ In contrast to extensive experimental diffusion data available for pure Pd, the information for CuPd alloys is limited. Diffusion measurements in the fcc Cu₄₇Pd₅₃ alloy using the Gorsky effect have been reported,¹³ and the activation barrier was found to be roughly 0.34 eV, compared with 0.23 eV in pure Pd. H diffusivity has also been measured using an electrochemical technique in CuPd alloys having compositions near the pure Pd limit at temperatures near room temperature and was found to slightly decrease with increasing Cu content.¹⁴ Experiments by Zetkin *et al.*^{30,31} for deuterium diffusion in the fcc phase of Cu₅₃Pd₄₇ and Cu₅₇Pd₄₃ alloys at temperatures between 600 and 800 K resulted in effective barriers of 0.34 and 0.35 eV, respectively.

Hydrogen diffuses through most metals and alloys by a series of discrete hops between interstitial binding sites.¹³ Lattice models are therefore a suitable choice for modeling long-range motion, where diffusion is described in terms of jump processes with an activation energy and prefactor depending on the chemical and physical structure of the initial and final sites. The difficulty in using such models lies in determining the relationships between the local structures of the many physically distinct binding sites and transition states in disordered alloys and the energies of these sites. A number of Monte Carlo studies of H diffusion in metal alloys using lattice models have been performed previously.^{15–18} For example, Brouwer *et al.* studied H diffusion in NbV alloys using a model defined using experimentally measured solubility data.¹⁹ Similarly, H diffusion was studied in AgPd alloys using Monte Carlo simulations based on a simplified model fitted to experimental diffusivities.²⁰ We aim to show

here that robust lattice models of H diffusion in metal alloys can be derived based on *ab initio* density functional theory (DFT) calculations of interstitial binding and motion. Unlike the models mentioned above, this approach does not require experimental data as input, so it is suitable for screening materials for which no reliable experimental data are available.

The paper is organized as follows. Section II describes our DFT calculations of H binding energies, vibrational frequencies, and hopping rates in two disordered fcc CuPd alloys with ~ 50 and 75 at. % Pd. The results from these extensive calculations are used to parametrize a lattice model for H diffusion in CuPd alloys with arbitrary alloy compositions greater than 47 at. % Pd. The dynamics of H diffusion in CuPd alloys can then be simulated at arbitrary temperatures and alloy compositions using a kinetic Monte Carlo (KMC) algorithm that is described in Sec. III. Section IV describes the temperature- and composition-dependent hydrogen diffusivities that are obtained from KMC simulations and compares these results to available experimental data. Our lattice model provides a straightforward means to study the potential impact of short-range order in CuPd alloys on H diffusion. This investigation is described in Sec. V, which indicates that the practical impact of short-range order in these materials on H diffusion is likely to be minimal. Section VI summarizes our results and discusses future applications of the methods we have introduced.

II. DFT METHODS

We performed plane-wave density functional theory calculations using the Vienna *ab initio* simulation package (VASP).^{21,22} The details of these calculations are similar to those reported previously.²³ These calculations examine material of infinite extent by using supercells with periodic boundary conditions in all three principal directions. Electron exchange-correlation effects were described using the generalized gradient approximation (GGA) with the Perdew-Wang 91 functional. Ion-electron interactions were described by the ultrasoft pseudopotentials (USPP's) introduced by Vanderbilt. A plane-wave expansion with a cutoff of 234 eV was used in all calculations. Total energy calculations used the residual minimization method for electronic relaxation accelerated using Methfessel-Paxton Fermi-level smearing with a width of 0.2 eV. Geometry relaxations were performed with a conjugate gradient method algorithm until the forces on all unconstrained atoms were less than 0.03 eV/Å. A Monkhorst-Pack mesh with a $4 \times 4 \times 4$ k grid was used for pure Pd calculations. In the case of the disordered fcc materials, a $2 \times 2 \times 2$ k grid was used for geometry relaxations, followed by a total energy calculation at the optimal geometry using a $4 \times 4 \times 4$ k grid for greater accuracy. All calculations used computational supercells of 27 metal atoms. For the disordered materials, atoms were randomly ordered within the supercell. While the use of a supercell inherently defines a material that is periodic on long length scales, the random ordering within the supercell provides a good approximation to the full range of local sites that exist in a completely randomly ordered material.

Since we aim to describe the properties of dilute interstitial H, calculations involving interstitial hydrogen were performed by placing a single H atom into the metallic supercell. This gives a H loading of $1/27$ relative to the PdH structure in which every octahedral site is occupied by H. In calculations involving H in pure Pd, all atoms in the computational supercell were fully allowed to relax during the calculations. In the case of interstitial H in CuPd, only the metal atoms adjacent to the H atom were relaxed during the calculations for computational efficiency. We have verified that further relaxation of outer metal atoms does not alter the energies obtained substantially. All calculations including interstitial H were performed for supercells with the lattice constant optimized using DFT prior to inserting H. The lattice expansions induced by H at dilute concentrations are small, so this is a reasonable approximation.

Transition states (TS's) for H diffusion in pure Pd and disordered CuPd alloys were determined using the dimer method.²⁴ To improve the efficiency of these calculations, we applied the dimer method to locate each TS in calculations using a single k point and subsequently recomputed the total energy of the TS using the larger k -point meshes listed above. During the dimer calculations, only the H atom was allowed to move, while keeping the metal atoms fixed. This was followed by relaxing the local metal atom geometry, while fixing the H atom at the estimated TS. This method had a significant computational advantage over allowing the H and local metal atoms to simultaneously relax during the calculation and gives an excellent approximation to the exact TS determined by the more time consuming direct calculation.

Zero-point energies (ZPE's) can be substantial for light interstitials such as H in metals. To quantify these energies, we calculated the normal-mode vibrational frequencies and associated zero-point energies of interstitial H at minima and transition states. The details of these calculations are described in our previous paper.²³

One means to compare the energy of interstitial H in alloys with differing compositions is to measure the binding energy of the interstitial species with respect to gaseous H_2 . Below we report classical binding energies defined by

$$E_b = E_{H/metal} - E_{metal} - \frac{1}{2}E_{H_2(g)}. \quad (1)$$

The terms on the right in this expression are the total energies of the supercell containing interstitial H, the supercell with no interstitial H, and an isolated H_2 molecule, respectively. With this definition, negative binding energies represent sites that are energetically preferred relative to gaseous hydrogen.

A. CuPd lattice constants

Equilibrium lattice constants were obtained using DFT for pure Pd, pure Cu, $Cu_{26}Pd_{74}$, and $Cu_{48}Pd_{52}$, giving 3.95 , 3.64 , 3.89 , and 3.83 Å, respectively. These are in good agreement with the corresponding experimental values for pure Pd, pure Cu, and $Cu_{48}Pd_{52}$ of 3.89 , 3.61 , and 3.77 Å (Refs. 11 and 12). The DFT-derived lattice constants are well described by

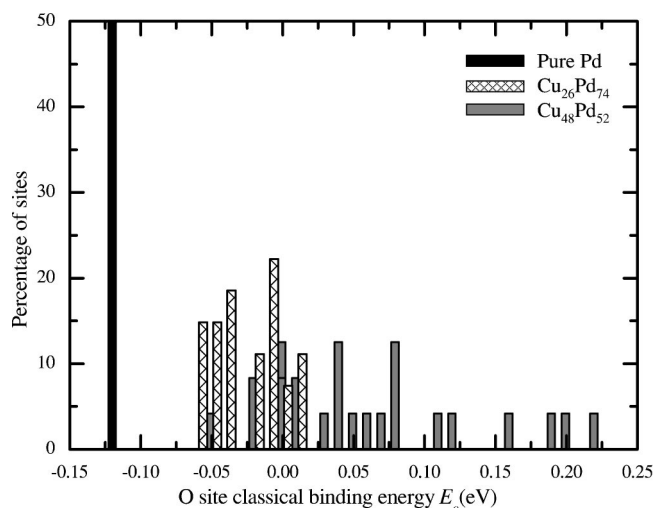


FIG. 1. Histogram of O-site classical binding energies in pure Pd, $\text{Cu}_{48}\text{Pd}_{52}$, and $\text{Cu}_{26}\text{Pd}_{74}$ as calculated using DFT.

a quadratic fit involving the alloy composition. This fit gives

$$a_0 = -0.11x_{Pd}^2 + 0.42x_{Pd} + 3.64, \quad (2)$$

where x_{Pd} is the atomic fraction of Pd in the alloy and a_0 is the lattice constant in Å. The lattice constant will be used below as a parameter implicitly linking the alloy composition to the binding energies at interstitial sites. The lattice constants defined by Eq. (2) show a positive deviation from Vegard's law, which predicts that a_0 varies linearly with x_{Pd} . The largest deviation occurs for $x_{Pd}=0.5$, where Eq. (2) gives $a_0=3.822$ Å and Vegard's law predicts $a_0=3.795$ Å.

B. Octahedral-site binding energies

In CuPd alloys, as in most fcc metals, interstitial H prefers to occupy octahedral (O) sites.^{25,26} We calculated the classical binding energies and ZPE's for all 27 O sites in our DFT supercells for $\text{Cu}_{48}\text{Pd}_{52}$ and $\text{Cu}_{26}\text{Pd}_{74}$ and also for pure Pd. A histogram of calculated classical binding energies for the three systems is presented in Fig. 1. The results for $\text{Cu}_{48}\text{Pd}_{52}$ and pure Pd have been presented before,²³ but are shown again here for completeness. The classical binding energy of the H atom is strongest in pure Pd, corresponding to a binding energy of -0.12 eV. In $\text{Cu}_{48}\text{Pd}_{52}$, binding energies ranged from -0.04 to $+0.21$ eV. In $\text{Cu}_{26}\text{Pd}_{74}$, E_b varied from -0.05 to $+0.01$ eV. The spread in the binding energy distribution is smaller for $\text{Cu}_{26}\text{Pd}_{74}$ than for $\text{Cu}_{48}\text{Pd}_{52}$ because there is less variation in the local environments defining the O sites in the former alloy.

To develop a model that can be applied to arbitrary alloy compositions, a simple way to express the binding energy in terms of the characteristics of an O site must be found. In general, a site binding energy depends on both the alloy lattice constant (composition) and metal-hydrogen interactions.²⁷ Furthermore, it is generally expected that metal-hydrogen interactions are short ranged,²⁷ suggesting that the composition of the shells of metal atoms surrounding an O site may give a satisfactory means to describe the observed variation in binding energies in Fig. 1. For each alloy,

we characterized all O sites by determining the number of Pd nearest neighbors (n_{NN} , $0 \leq n_{NN} \leq 6$) and Pd next nearest neighbors (n_{NNN} , $0 \leq n_{NNN} \leq 8$). Examining the site energies for each alloy separately as a function of n_{NN} and n_{NNN} suggests that E_b decreased as n_{NN} became larger and increased with increasing n_{NNN} . This suggests that the strongest binding sites have a large n_{NN} —i.e., $n_{NN} \geq 4$ —and small n_{NNN} —i.e., $n_{NNN} \leq 1$.

The 27-atom supercell used for our DFT calculations provides a representative sampling of sites that would be observed in substitutionally random alloy. Only a small number of these sites have the characteristics of the strong binding sites identified above. The strong binding sites are, however, crucial in the determination of dilute H solubility and diffusivity. In light of this observation, we performed additional DFT calculations to describe these strong binding sites more completely in the $\text{Cu}_{48}\text{Pd}_{52}$ alloy. To create strong binding sites, we focused on a single O site with $n_{NN}=4$ and $n_{NNN}=2$. We then swapped the positions of atoms in the nearest-neighbor, next-nearest-neighbor, and if necessary, third-neighbor shells with other atoms in the supercell while keeping the overall alloy composition fixed. For example, to obtain a site with a local configuration of $n_{NN}=5$ and $n_{NNN}=1$, the position of a Cu atom in the nearest-neighbor shell was exchanged with a Pd atom from the next-nearest-neighbor shell. Proceeding in this way, we calculated the binding energies for sites with the following local environments: $n_{NN}=4$ and $n_{NNN}=0$, $n_{NN}=5$ and $n_{NNN}=0$, $n_{NN}=6$ and $n_{NNN}=0$, $n_{NN}=5$ and $n_{NNN}=1$, and $n_{NN}=6$ and $n_{NNN}=1$. The binding energy of all these sites was approximately the same, between -0.06 and -0.07 eV, suggesting that binding energy saturates as the local environment moves toward what was identified above as the most favorable type of binding site.

Combining all of our DFT-calculated binding energies allowed us to seek a simple model to correlate the observed binding energies with alloy composition and the binding site's local environment. The entire data set calculated above was combined and fit to a functional form containing n_{NN} , n_{NNN} , and a_0 . A simple linear dependence of the octahedral site binding energy, E_O (eV), on n_{NN} , n_{NNN} , and a_0 (Å) was found to yield a good fit:

$$E_O = -0.020n_{NN} + 0.024n_{NNN} - 1.42a_0 + 5.45. \quad (3)$$

A plot of binding energies obtained using Eq. (3) is compared with our DFT results in Fig. 2. The absolute deviation between Eq. (3) and the DFT results ranged from 0 to 0.07 eV, with most data points having an absolute deviation less than 0.03 eV from the DFT values. As an example, the classical binding energy of pure Pd calculated using Eq. (3) is -0.09 eV, while DFT gives -0.12 eV. There is considerable scatter in Fig. 2. We tested several alternatives to Eq. (3) that included, for example, parameters that described the spatial arrangement of Pd nearest neighbor atoms. All of these alternate fitting functions involved more adjustable parameters than Eq. (3), but none reduced the scatter in plots analogous to Fig. 2 sufficiently to make them preferable to Eq. (3).

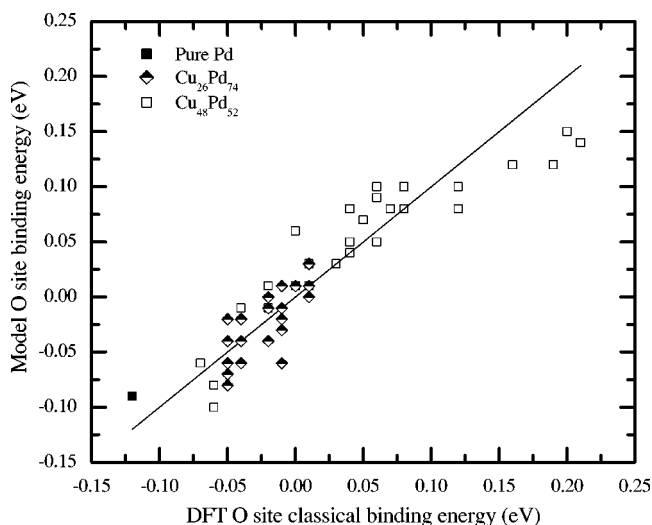


FIG. 2. Scatter plot comparing O-site classical binding energies calculated using DFT and predicted using Eq. (3).

C. Tetrahedral-site binding energies

The tetrahedral (T) sites in fcc CuPd alloys also define locally stable binding sites for interstitial H. We used DFT to calculate the T-site classical binding energies for pure Pd and all 54 possible sites in the supercells of CuPd alloys. The T-site binding energy in pure Pd is 0.05 eV higher in energy than the O site. The T-site binding energies of $\text{Cu}_{48}\text{Pd}_{52}$ and $\text{Cu}_{26}\text{Pd}_{74}$ are summarized in Fig. 3. The distribution of binding energies is narrower for $\text{Cu}_{26}\text{Pd}_{74}$, similar to that observed for O sites. Expressions similar to Eq. (3) were not able to correlate the DFT-calculated T-site binding energies in a satisfactory manner. To describe the T-site binding energies in a parametric model, we calculated the mean classical binding energy $E_{b,mean}$ as a function of n_{NN} ($0 \leq n_{NN} \leq 4$) for each alloy and pure Pd. $E_{T,mean}$ (eV) was fitted to a linear function consisting of n_{NN} and a_0 (Å):

$$E_{T,mean} = -0.019n_{NN} - 1.74a_0 + 6.89. \quad (4)$$

The variation of energies around $E_{T,mean}$ was modeled using a Gaussian distribution with standard deviation σ (eV). The

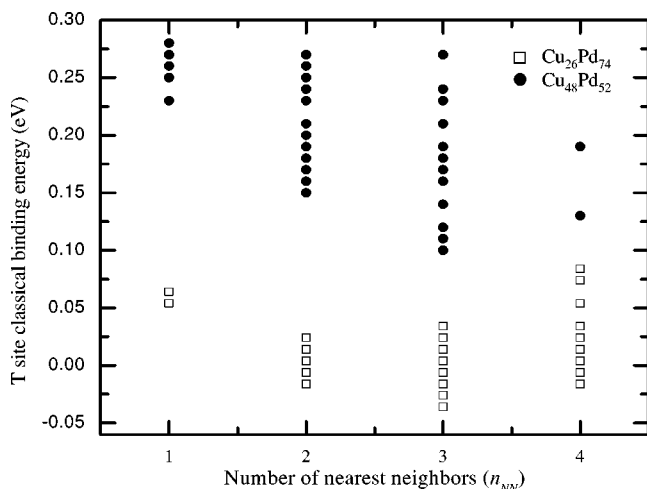


FIG. 3. T-site classical binding energies calculated using DFT for $\text{Cu}_{48}\text{Pd}_{52}$ and $\text{Cu}_{26}\text{Pd}_{74}$.

variation in T-site binding energies in our DFT results is well described by using

$$\sigma = 0.033 \frac{4!}{n_{NN}! (4 - n_{NN})!} x_{Pd}. \quad (5)$$

D. Diffusion activation barriers

Interstitial H diffuses in fcc CuPd alloys by thermally activated hops between an O site and T site. Classical rate theory cannot be applied directly to determine the transition rate between adjacent binding sites, since in its derivation the possible energy levels are assumed to form a continuum.¹³ The hopping rates can be described in a way that incorporates the discrete energy levels available to interstitial H by using the following quantum mechanically modified version of classical harmonic transition-state theory:²⁸

$$k_{OT} = \Gamma_{OT} \exp(-E_d/kT), \quad (6)$$

where

$$\Gamma_{OT} = \frac{\prod_{i=1}^3 \nu_{O,i} f(h\nu_{O,i}/2kT)}{\prod_{j=1}^2 \nu_{TS,j} f(h\nu_{TS,j}/2kT)}. \quad (7)$$

In these expressions, k_{OT} is the hopping rate from an O to a T site, $f(x) = \sinh(x)/x$, $\nu_{O,i}$ ($\nu_{TS,i}$) are the frequencies at the O (TS) site, and E_a is the classical activation barrier. A similar expression applies to the T to O hopping rate k_{TO} . This description assumes that lattice vibrations can be decoupled from the localized H vibrations and that the potential energy surfaces for H in the vicinity of the minima and TS can be approximated as harmonic. These two assumptions were also made in our DFT calculations of the H vibrational frequencies. In the high-temperature limit where $h\nu \ll kT$, the classical limit corresponding to the frequency product of Vineyard²⁹ is obtained. In the low-temperature limit, the effective activation energy defined by Eqs. (6) and (7) reduces to the zero-point-corrected values we used in our earlier work.²³

Due to the disordered nature of CuPd alloys, there are a large number of intersite hopping barriers in these materials. Directly determining barriers for all possible hopping pathways in the supercells treated using DFT is currently computationally infeasible. In our previous work,²³ we used the dimer method to estimate the activation barriers for pure Pd and a few representative sites in $\text{Cu}_{48}\text{Pd}_{52}$. In the case of pure Pd, the energy at the TS was 0.12 eV higher than the corresponding T site. We extended this study to perform a more detailed analysis of activation barriers in $\text{Cu}_{48}\text{Pd}_{52}$ and $\text{Cu}_{26}\text{Pd}_{74}$. The aim of this analysis was to parametrize E_a in a manner similar to that used above for the binding energies for O and T sites. We located the TS and classical E_a for ten representative O-T pathways in each alloy treated with DFT. Our results show that average value of $(E_{TS} - E_T)$ was 0.14 ± 0.02 eV for $\text{Cu}_{48}\text{Pd}_{52}$ and 0.13 ± 0.02 eV for $\text{Cu}_{26}\text{Pd}_{74}$. The mean values of $(E_{TS} - E_T)$ for these two CuPd alloys and pure Pd can be described by a simple linear function of x_{Pd} :

TABLE I. Zero-point energies and normal-mode frequencies at O, T, and TS used to model alloy compositions between 40 at. % Pd and 100 at. % Pd.

Parameter	Composition (at. % Pd)	ZP Energy (eV)	ν (10^{13} s $^{-1}$)
$\nu_{O,i}$	90–100	0.09	0.93, 0.93, 0.93
	75–90	0.10	1.73, 1.84, 1.42
	60–74	0.11	1.73, 1.87, 1.89
	40–59	0.12	1.41, 2.46, 1.71
$\nu_{T,i}$	40–100	0.19	3.73, 1.88, 3.59
$\nu_{TS,i}$	40–100	0.17	3.89, 4.16

$$E_{TS} - E_T = -0.04x_{Pd} + 0.16. \quad (8)$$

The activation energy for an O to T hop can therefore be written as

$$E_a = E_T - E_O - 0.04x_{Pd} + 0.16. \quad (9)$$

In Eqs. (8) and (9), all energies are in eV.

E. Diffusion prefactors

To apply Eqs. (6) and (7), the normal mode frequencies of interstitial H at local binding sites and transition states must be estimated. We used DFT to calculate the H vibrational frequencies and associated zero-point energies in representative sites in Cu₄₈Pd₅₂ and Cu₂₆Pd₇₄. The mean O-site ZP energy for Cu₂₆Pd₇₄ and Cu₄₈Pd₅₂ was found to be 0.11 and 0.12 eV, respectively. The analogous ZP energy for pure Pd was 0.09 eV. The ZP energies at the T sites in all three materials were found to be ~ 0.19 eV. Similarly, the ZP energies of all the TS we examined in these three materials were ~ 0.17 eV.

To define the normal-mode frequencies in Eq. (7) in a form suitable for our lattice model, we assumed that $\nu_{TS,i}$ and $\nu_{T,i}$ were independent of alloy composition. The O-site frequencies $\nu_{O,i}$ were assumed to be constant over moderate ranges of alloy composition. These frequencies are summarized in Table I.

The discussion above completely defines a lattice model for the binding and hopping of interstitial H at dilute concentrations in CuPd alloys of arbitrary composition with $x_{Pd} \geq 0.5$. This model can be summarized as follows. Once the identity of each Pd and Cu atom in a disordered fcc lattice has been defined, the H binding energy in each O site is defined by Eq. (3). The T-site binding energies are defined by Eqs. (4) and (5). Once the Gaussian contribution to the T-site binding energy defined by Eq. (5) is assigned randomly to each site, the T-site energies are fixed for further applications of the structure. After the O- and T-site energies are defined in this way, the O-to-T and T-to-O hopping rates are defined by Eq. (6) using the activation energies defined by Eqs. (8) and (9) with the local vibrational frequencies shown in Table I.

III. KMC SIMULATIONS

The model summarized above defines the local hopping rates of interstitial H atoms. The long-range mobility of H atoms in arbitrary alloy structures can be examined numerically using kinetic Monte Carlo simulations. We used the following KMC algorithm to follow the time evolution of non-interacting H atoms in CuPd alloys. At each step in our KMC algorithm, an interstitial H atom is selected randomly from all H atoms in the simulation volume and a move direction from current site is selected randomly from the 8 (4) directions available for an O (T) site. Because all T-to-O hops in our model, for a given alloy composition, have the same rate and this rate is faster than all O-to-T hops, T-to-O hops are accepted with probability 1. Hops that move an atom from an O site to a T site are accepted with probability $2k_{OT}/k_{TO}$. The factor of 2 in this acceptance probability arises because of the different number of hopping directions available to the two types of sites. Regardless of the outcome of the attempted hop, time is incremented by $\Delta t = 1/4Nk_{TO}$, where N is the total number of interstitial atoms in the simulation volume. It is straightforward to show that this algorithm correctly defines the local hopping rates of all possible processes in our lattice model. We have not included site blocking effects in our simulations since we are interested in dilute H concentrations, but it would be straightforward to include these effects in our simulations.

To measure the diffusivity of interstitial H in our lattice model, we used simulation cells with 2048 metal atoms randomly distributed on an fcc lattice with a chosen overall alloy composition. We verified that using 2048 metal atoms was sufficient to yield results that are not affected by finite-size effects by comparing our calculations with simulations for larger volumes. In each simulation, 150 H atoms were initially distributed randomly among the O and T sites of the lattice. A large number of KMC steps (typically > 5000 MC steps per H atom) were then used to thermally equilibrate the system. After equilibration, a further 50 000 MC steps per H atom were performed while collecting data on the trajectory of each atom. The tracer diffusivity of the H atoms was then computed using the usual Einstein expression

$$D_s = \lim_{t \rightarrow \infty} \left[\frac{1}{6Nt} \sum_{i=1}^N \langle |R_i(t) - R_i(0)|^2 \rangle \right]. \quad (10)$$

Here, the vector $R_i(t)$ determines the position of an atom at time t and the angular brackets denote an average over all mobile atoms.

IV. H DIFFUSION IN CuPd ALLOYS

We performed KMC simulations as described above to calculate the tracer diffusivity of H atoms in CuPd alloys with compositions ranging from $0.5 \leq x_{Pd} \leq 1$ at temperatures from 400 to 1200 K. An Arrhenius plot of D_s as a function of T for the entire range of x_{Pd} and T is shown in Fig. 4. At $T=400$ K, D_s ranged from 8.11×10^{-10} m²/s for pure Pd to 1.32×10^{-11} m²/s at $x_{Pd}=0.5$, differing by a factor of ~ 60 . At the highest temperature we examined, $T=1200$ K, D_s var-

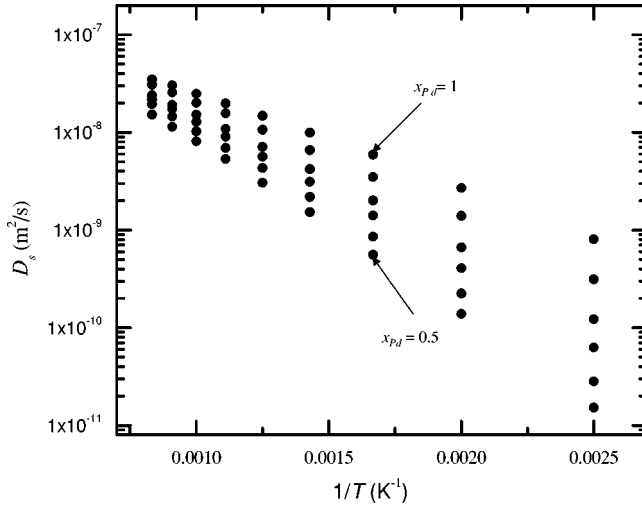


FIG. 4. Arrhenius plot of D_s as a function of T for pure Pd (top plot) and fcc CuPd alloys with compositions $x_{Pd}=0.9, 0.8, 0.7, 0.6, 0.5$ (in descending order).

ied only by a factor of ~ 2.2 between $2.87 \times 10^{-8} \text{ m}^2/\text{s}$ for Pd and $1.32 \times 10^{-8} \text{ m}^2/\text{s}$ at $x_{Pd}=0.5$.

As expected, the temperature dependence of the H diffusivity in each alloy can be represented by

$$D_s = D_0 \exp(-E_{a,eff}/kT), \quad (11)$$

where D_0 and $E_{a,eff}$ are the diffusion prefactor and effective activation barrier, respectively. The plots shown in Fig. 4 possess some curvature, which results from both the behavior of the quantum-corrected rate equations used to define our model and from the structural heterogeneity of the materials in which H is diffusing. Instead of extracting a single D_0 and $E_{a,eff}$ for the entire range of T , we applied Eq. (11) separately to the moderate ($T < 700 \text{ K}$) and high ($T > 1000 \text{ K}$) temperature ranges. The results of this fitting procedure are shown in Table II. At moderate T , $E_{a,eff}$ decreases as x_{Pd} increases and varies from 0.37 eV at $x_{Pd}=0.50$ to 0.21 eV in pure Pd. The same values for the high- T range were lowered to 0.33 eV at $x_{Pd}=0.50$ and 0.17 eV in pure Pd. Overall, we find that the values of the

TABLE II. Arrhenius prefactors D_0 and effective barriers $E_{a,eff}$ for moderate T ($T < 700 \text{ K}$) and high T ($T > 1000 \text{ K}$) for pure Pd and CuPd alloys as determined from the results in Fig. 4.

x_{Pd}	Moderate T		High T	
	D_0 ($10^{-7} \text{ m}^2 \text{ s}^{-1}$)	$E_{a,eff}$ (eV)	D_0 ($10^{-7} \text{ m}^2 \text{ s}^{-1}$)	$E_{a,eff}$ (eV)
1	3.10	0.21	1.77	0.17
0.9	4.27	0.25	2.22	0.21
0.8	5.11	0.29	2.37	0.24
0.7	6.47	0.32	2.87	0.28
0.6	7.18	0.35	3.77	0.32
0.5	6.81	0.37	3.04	0.33

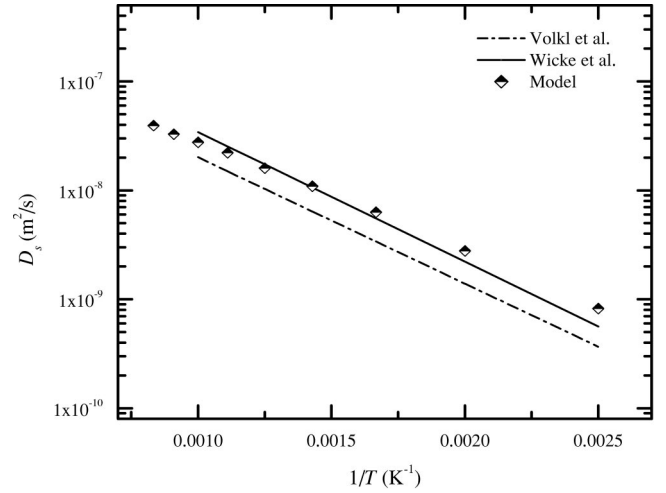


FIG. 5. Arrhenius plot of D_s as a function of T for pure Pd shown for model and experimental data. The two solid lines are fits to experimental data by Volkl and Alefield (Ref. 13) and Wicke and Brodowsky (Ref. 26).

prefactors tend to decrease with x_{Pd} . The fcc alloy with $x_{Pd}=0.50$ is only metastable in the moderate temperature regime, since a bcc structure can be favored under these conditions. For all the other conditions addressed by our simulations, the fcc alloy is the stable CuPd alloy.

H diffusion in pure Pd at dilute loadings has been extensively studied experimentally. A compilation of several sets of experimental results at low and moderate temperatures by Volkl and Alefield¹³ showed a remarkable consistency in the data and was combined to yield a fit with $D_0=2.9 \times 10^{-7} \text{ m}^2/\text{s}$ and $E_{a,eff}=0.23 \text{ eV}$. The results of experiments by Wicke and Brodowsky²⁶ gave a fit of $D_0=5.3 \times 10^{-7} \text{ m}^2/\text{s}$ and $E_{a,eff}=0.24 \text{ eV}$. These fits were obtained by using data over the entire temperature range and do not treat the high-temperature behavior separately. Figure 5 shows a comparison of diffusivities obtained using the model and these fits to experimental data. The diffusion coefficients from simulation are in good agreement with experimental results. At the lowest temperatures studied, the model overpredicts experimental values by a factor of ~ 2 or less. For high temperatures, our model diffusivities lie in between the two experimental sets of results. The moderate- T activation barrier from our model of 0.21 eV in pure Pd agrees well with the experimental barriers discussed above.

Compared to pure Pd, there is limited experimental diffusion data for CuPd alloys. Gorsky effect experiments¹³ for $\text{Cu}_{47}\text{Pd}_{53}$ at temperatures ranging from 290 to 500 K resulted in $E_{a,eff}=0.35 \text{ eV}$ and $D_0=2.65 \times 10^{-7} \text{ m}^2/\text{s}$. Our model gives $E_{a,eff}=0.37$ and $D_0=6.79 \times 10^{-7} \text{ m}^2/\text{s}$ for $x_{Pd}=0.50$ in the temperature range where the fcc alloy is stable at this composition. For example at $T=500 \text{ K}$, the theoretical and experimental diffusivity was $1.01 \times 10^{-10} \text{ m}^2/\text{s}$ and $1.00 \times 10^{-10} \text{ m}^2/\text{s}$, respectively. At $T=300 \text{ K}$, the theoretical and experimental diffusivity was $4.59 \times 10^{-13} \text{ m}^2/\text{s}$ and $3.30 \times 10^{-13} \text{ m}^2/\text{s}$, respectively. We also calculated deuterium diffusion coefficients in $\text{Cu}_{53}\text{Pd}_{47}$ and $\text{Cu}_{57}\text{Pd}_{43}$ at temperatures between 600 and 850 K, corresponding to the experimental conditions used by Zetkin *et al.*^{30,31} For the

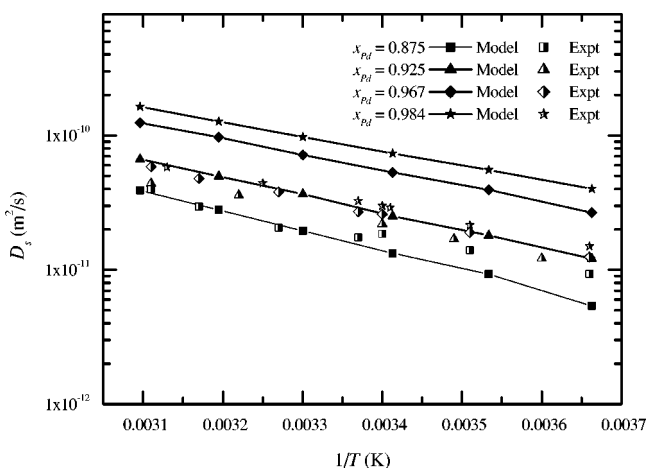


FIG. 6. D_s as a function of T for Pd-rich CuPd alloys at $x_{Pd}=0.875, 0.925, 0.967, 0.984$ as determined by our simulations (symbols connected by lines) and experimental data from Kircheim and McLellan (Ref. 14) (half solid symbols).

$\text{Cu}_{53}\text{Pd}_{47}$ alloy, the theoretical and experimental barriers were both 0.34 eV. The theoretical and experimental diffusivity was $1.62 \times 10^{-9} \text{ m}^2/\text{s}$ and $1.17 \times 10^{-9} \text{ m}^2/\text{s}$, respectively, at $T=700 \text{ K}$. Similarly for the $\text{Cu}_{57}\text{Pd}_{43}$ alloy, the theoretical barrier of 0.36 eV agreed well with the experimental value of 0.35 eV. The theoretical diffusivity at $T=700 \text{ K}$ was $1.42 \times 10^{-9} \text{ m}^2/\text{s}$, overpredicting the experimental value of $6.14 \times 10^{-10} \text{ m}^2/\text{s}$. Kircheim and McLellan¹⁴ measured H diffusivities at dilute loadings in four Pd-rich CuPd alloys ($x_{Pd}=0.875, 0.925, 0.967, 0.984$) over a small range of temperatures, 273–323 K. We performed KMC simulations at the same compositions and temperatures as the above experiments. The results of our simulations are presented in comparison with experimental data in Fig. 6. Consistent with the results in Fig. 5, our model overpredicts the diffusivity of H in alloys that are almost pure Pd in this temperature range. Our model correctly predicts that the H diffusivity decreases as the Pd content in the alloy decreases, although the strength of this effect is overestimated by the model. From Figs. 5 and 6 we can conclude that our model describes H diffusion in fcc CuPd alloys with semi-quantitative accuracy. Since the model was determined directly from ab *initio* data and did not involve any fitting to experimental data, this outcome suggests that the methods we have used here may be quite useful in screening materials for which experimental data is not available.

V. EFFECTS OF SHORT-RANGE ORDER IN CuPd ALLOYS

Binary alloys often form solid solutions in which the atoms are not randomly arranged, but may instead possess some extent of short-range order (SRO).³² The presence of local order can have a major effect on various physical and chemical properties of the alloys.³³ SRO is typically quantified using the Warren-Cowley parameter α_j defined by³²

$$\alpha_j = 1 - \frac{P_{\text{Cu}(\text{Pd})}^j}{x_{\text{Pd}}} \quad (12)$$

Here, $P_{\text{Cu}(\text{Pd})}^j$ is the conditional probability that given a Cu atom at the origin, there is a Pd atom at the j th-neighbor distance. The sign of α_j indicates whether atoms in a given distance j prefer Cu-Pd ordering ($\alpha_j < 0$) or clustering ($\alpha_j > 0$). The Warren-Cowley parameters are normalized such that $-1 \leq \alpha_j \leq 1$, and $\alpha_j = 0$ represents a substitutionally random alloy. SRO in Cu-rich CuPd alloys has been the subject of extensive experimental and theoretical study.³⁴ For alloys with $x_{Pd}=0.10-0.40$, which surround the ordered Cu_3Pd structure,^{11,12} values of α_1 are in the range -0.18 to -0.1 (Ref. 34). We know of no evidence of local ordering in CuPd alloys at the composition and temperature range studied in this work. However, we chose to study the effects of short-range order on H diffusivities using CuPd alloys as a prototypical system with the aim of understanding the qualitative effects of SRO on H diffusion in binary alloys. We restricted our attention to chemical ordering with respect to the nearest-neighbor shell ($j=1$) in two representative alloys with $x_{Pd}=0.50$ and 0.75 .

We used a reverse Monte Carlo (RMC) algorithm to create various alloy structures possessing short-range order. Using a randomly generated lattice similar to those in our previous calculations ($\alpha_1 \cong 0$) as a starting point, we generated a series of structures with an ordering tendency ($\alpha_1 < 0$). Similarly, alloys with a tendency to form clusters of like atoms were created from an initial configuration of a nearly segregated lattice divided into Cu and Pd domains with a common interface. During the RMC simulation, a trial move consisted of choosing a random pair of atoms in the lattice and attempting to swap their positions. All moves causing α_1 to move closer to the target value (α_{targ}) were accepted with probability of unity, and a fraction of the remaining moves were accepted with a probability $\exp(-\beta|\alpha_1 - \alpha_{\text{targ}}|)$, with β as an adjustable parameter. The value of β was adjusted for each value of α_{targ} and ranged from 0.005 to 0.009. This procedure was used to generate alloys with α_1 ranging from -0.3 to 0.7 . As an example, a fully segregated alloy structure with 2048 atoms consisting of Cu and Pd domains separated by an interface had $\alpha_1=0.79$ at $x_{Pd}=0.5$ and $\alpha_1=0.75$ at $x_{Pd}=0.75$. Furthermore, $\alpha=-0.33$ is found for a system with Pd_2Cu_2 stoichiometry at $x_{Pd}=0.5$, represented using a four-atom cubic fcc unit cell with Cu atoms in the corner and one face center and two Pd atoms in the remaining face centers. Similarly at $x_{Pd}=0.75$, the value $\alpha_1=-0.33$ also corresponded to an ordered system with Pd_3Cu stoichiometry, whose cubic fcc unit cell consisted of a Cu atom at a corner and three Pd atoms at the face centers.

For values of α_1 where significant segregation occurs, clusters containing purely Cu and Pd atoms appear in the lattice. These clusters will most likely possess different properties than the remaining regions of the alloy. It is crucial to model these clusters in an appropriate manner to yield physically reasonable binding energies and barriers during the simulation. In our KMC simulations of alloys with SRO, O, and T sites for which all of the nearest and next-nearest

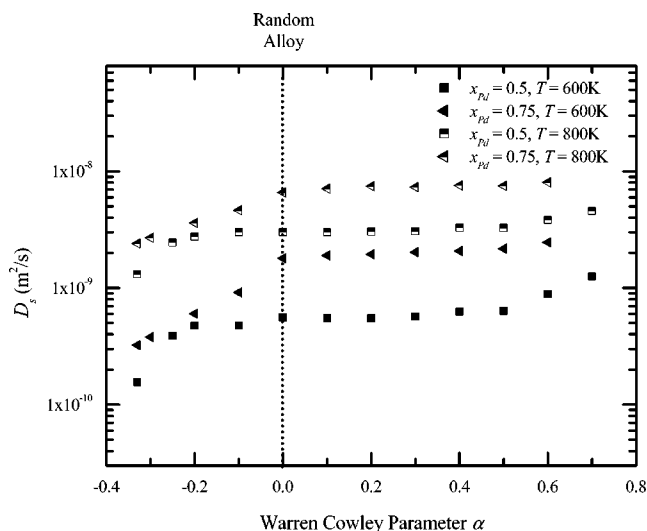


FIG. 7. Predicted tracer diffusivity, D_s , as a function of the Warren-Cowley parameter, α_1 , for CuPd alloys with two alloy compositions at $T=600$ and 800 K.

neighbors were the same metallic species were identified. For these sites, the lattice parameter was set to be the mean of the pure metal and alloy values defined by Eq. (2).

H diffusivities for diffusion in the structures containing SRO were calculated using KMC for temperatures ranging from 400 to 1200 K. A representative plot of D_s as a function of α_1 is shown for $T=600$ K and 800 K in Fig. 7. Results for other temperatures were similar. For $\alpha_1 > 0$, the diffusivities remain nearly constant over a wide range of positive values. As α_1 approaches 0.70, the number of pure Pd clusters increases and these clusters are highly favorable for interstitial H. The diffusion in this limit is dominated by hops within the pure Pd clusters, causing an increase in D_s as α_1 increases further. When $\alpha_1 < 0$, D_s decreases as α becomes more negative and eventually approaches the values for the stoichiometric structures described above at $\alpha_1 = -0.33$. These results highlight the fact that simple ordered structures, in general, do not give good approximations to the diffusion rates of interstitial H in substitutionally random alloys.

Our results allow us to draw a useful conclusion regarding the applicability of our results from substitutionally random alloys to real CuPd alloys that may have limited SRO. Typical α values found experimentally in disordered transition-metal alloys range from -0.1 to 0.4 (Refs. 32 and 35). Therefore, we conclude that short-range ordering has at worst a minimal impact on the diffusion rates of H in fcc CuPd alloys.

VI. CONCLUSION

We developed a lattice-gas model derived solely from first-principles calculations and successfully applied it to quantitatively predict H tracer diffusivities in fcc CuPd alloys for a wide range of compositions and temperatures. DFT calculations were used to characterize the binding energies, zero-point energies, and activation barriers for H in a

representative sampling of interstitial sites in $\text{Cu}_{48}\text{Pd}_{52}$ and $\text{Cu}_{26}\text{Pd}_{74}$. These results were used to define a lattice model that accounts for all possible local hopping rates for alloys with $x_{\text{Pd}} > 0.47$. KMC simulations performed at temperatures ranging from 400 to 1200 K showed that the H diffusivity decreased as a function of increasing Cu content in the alloy, consistent with experimental observations. At high temperatures, the dependence of the diffusivity on alloy composition becomes weak. This means that at high T the diffusion coefficients in most of the fcc CuPd alloys will be comparable to pure Pd.

We have previously argued that the effective activation barrier to H diffusion in a disordered metal alloy can be estimated by determining the activation energy for local hopping out of the interstitial sites that bind H most favorably.²³ Applying this argument to $\text{Cu}_{48}\text{Pd}_{52}$, we suggested that 0.27 eV as a lower bound on the effective barrier. The simulations presented here allow the accuracy of this crude estimate to be examined. The results of our KMC simulations indicate that the effective activation energy for this alloy is 0.33 – 0.37 eV, depending on the temperature range of interest. Thus, while it is correct to say that our previous estimate was a lower bound on the actual result, this estimate was substantially lower than the true result. The origin of this underestimation is straightforward to understand. Our estimate examined only local hops out of energetically favorable sites. This process is clearly a prerequisite for long-range diffusion, but long-range diffusion also requires the diffusing H atom to overcome additional barriers separating somewhat less favorably binding sites. Despite the physical simplicity of this picture, it is not simple to refine the estimate of the effective activation energy based solely on isolated barriers computed using DFT. The lattice model and associated KMC simulations that we have discussed in this paper provide a direct means to determine the effective activation energy associated with the full energy landscape explored by diffusing H.

One area for potential refinement of the approach we have presented here lies in the formulation of the lattice model. An important constraint on any formulation of these models is that they rely only on information that is easily defined from lattice representations of the alloy. For example, information regarding the local electronic density of states in interstitial sites cannot be incorporated into a lattice model unless this information can be correlated in some way with the local structure of the sites. One minor aspect of our lattice model that we explored was our approach of defining the binding energy of T sites using both a mean value and a randomly assigned contribution [see Eqs. (4) and (5)]. We tested models that neglected the random portion of this energy and found that the resulting diffusivities differed negligibly from those computed using the full model.

Another area for model improvement would be to use more rigorous methods to incorporate anharmonic effects while modeling H vibrations. These effects can be treated using perturbative and Fourier expansion methods, as has been done previously for pure Pd.³⁶ A significant difficulty with this direction is that treating anharmonic effects requires a far more detailed characterization of the potential energy surface than is needed in the harmonic assumptions we have

used. Since we are particularly interested in disordered alloys where large numbers of locally distinct sites must be examined, use of calculation methods that greatly increase the computational effort required for each site would represent a significant challenge. We feel that the methods we have described here are a useful compromise between accuracy and feasibility for structurally complex materials.

Our results illustrate the power of our model as a predictive tool to accurately determine H diffusivity over a broad range of temperature and composition in disordered metal

alloys. Calculations of this nature should prove to be a useful complement to experimental studies in efforts to select metal alloys with favorable diffusion properties for H for a variety of applications.

ACKNOWLEDGMENT

This work was partially supported by the ACS Petroleum Research Fund.

*Corresponding author. Electronic address: sholl@andrew.cmu.edu

- ¹L. Schlapbach and A. Züttel, *Nature (London)* **414**, 353 (2001).
- ²Y. S. Cheng *et al.*, *J. Membr. Sci.* **204**, 329 (2002).
- ³B. D. Morreale *et al.*, *J. Membr. Sci.* **212**, 87 (2003).
- ⁴D. J. Edlund and W. A. Pledger, *J. Membr. Sci.* **77**, 255 (1993).
- ⁵D. J. Edlund *et al.*, *Gas Sep. Purif.* **8**, 131 (1994).
- ⁶N. Lopez and J. K. Norskov, *Surf. Sci.* **477**, 59 (2001).
- ⁷F. Roa *et al.*, *Chem. Eng. J.* (to be published).
- ⁸F. Roa, M. J. Block, and J. D. Way, *Desalination* **147**, 411 (2002).
- ⁹S. E. Nam and K. H. Lee, *J. Membr. Sci.* **192**, 177 (2001).
- ¹⁰T. L. Ward and T. Dao, *J. Membr. Sci.* **153**, 211 (1999).
- ¹¹W. B. Pearson, *A Handbook of Lattice Spacings and Structures of Metals and Alloys* (Macmillan, New York, 1958).
- ¹²M. Hansen, *Constitution of Binary Alloys* (McGraw-Hill, New York, 1958).
- ¹³J. Volkl and G. Alefeld, in *Hydrogen in Metals I*, edited by G. Alefeld and J. Volkl (Springer-Verlag, Berlin, 1978), Vol. 28, p. 321.
- ¹⁴R. Kirchheim and R. B. McLellan, *Acta Metall.* **28**, 1549 (1980).
- ¹⁵K. W. Kehr and T. Wichmann, *Mater. Sci. Forum* **223**, 151 (1996).
- ¹⁶K. W. Kehr and O. Paetzold, *Physica A* **190**, 1 (1992).
- ¹⁷R. Kirchheim, *Defect Diffus. Forum* **143**, 911 (1997).
- ¹⁸L. F. Perondi, R. J. Elliott, and K. Kaski, *J. Phys.: Condens. Matter* **38**, 7949 (1997).
- ¹⁹R. C. Brouwer, E. Salomons, and R. Griessen, *Phys. Rev. B* **38**,

10 217 (1988).

- ²⁰H. Barlag, L. Opara, and H. Zuchner, *J. Alloys Compd.* **330–332**, 434 (2002).
- ²¹G. Kresse and J. Hafner, *Phys. Rev. B* **48**, 13 115 (1993).
- ²²G. Kresse and J. Furthmüller, *Comput. Mater. Sci.* **6**, 15 (1996).
- ²³P. Kamakoti and D. S. Sholl, *J. Membr. Sci.* **225**, 145 (2003).
- ²⁴G. Henkelman and H. Jonsson, *J. Chem. Phys.* **111**, 7010 (1999).
- ²⁵J. Volkl and G. Alefeld, in *Hydrogen in Metals 2*, edited by G. Alefeld and J. Volkl (Springer-Verlag, Berlin, 1978), p. 11.
- ²⁶E. Wicke and H. Brodowsky, in *Hydrogen in Metals 2* (Ref. 25), p. 73.
- ²⁷R. C. Brouwer and R. Griessen, *Phys. Rev. B* **40**, 1481 (1989).
- ²⁸L. Katz, M. Guinan, and R. J. Borg, *Phys. Rev. B* **4**, 330 (1971).
- ²⁹G. H. Vineyard, *J. Phys. Chem. Solids* **3**, 121 (1957).
- ³⁰A. S. Zetkin, G. Y. Kagan, and E. S. Levin, *Phys. Met. Metallogr.* **64**, 130 (1987).
- ³¹A. S. Zetkin, G. E. Kagan, and A. N. Varakshin, *Sov. Phys. Solid State* **34**, 83 (1992).
- ³²S. Müller, *J. Phys.: Condens. Matter* **15**, R1429 (2002).
- ³³G. E. Ice and C. J. Sparks, *Annu. Rev. Mater. Sci.* **29**, 25 (1999).
- ³⁴R. V. Chepul'skii, J. B. Staunton, E. Bruno, B. Ginatempo, and D. D. Johnson, *Phys. Rev. B* **65**, 064201 (2002).
- ³⁵C. Wolverton, V. Ozolins, and A. Zunger, *Phys. Rev. B* **57**, 4332 (1998).
- ³⁶C. Elsasser *et al.*, *J. Phys.: Condens. Matter* **4**, 5207 (1992).